Mapping Multivariate Influence of Alloying Elements on Creep Behavior for Design of New Martensitic Steels

AMIT K. VERMA, JEFFERY A. HAWK, LAURA S. BRUCKMAN, ROGER H. FRENCH, VYACHESLAV ROMANOV, and JENNIFER L.W. CARTER

Heritage data for the class of 9 to 12 wt pct Cr steels are studied using data science to quantify the statistically significant relationships among multiple processing/microstructure and performance variables. The effort is undertaken to find new martensitic steels for creep life of 10^5hours or greater at 650 °C and 100 MPa using machine learning. Linear regression and lasso regression were utilized to identify alloying elements that contribute towards better creep strength. Visualization techniques such as t-distributed stochastic neighbor embedding and pair-wire element specific comparisons were utilized to explore information gaps that exist within the data and are in conflict with existing domain knowledge. Combining all results suggest that the next alloy design to be explored should be 9 wt pct Cr with high W (2 to 3 wt pct) and high Co (2 to 3 wt pct) for creep life of 10^5 hours or greater at 650 °C, 100 MPa.

https://doi.org/10.1007/s11661-019-05234-9

I. INTRODUCTION

SIXTY-THREE percent of U.S. electricity generation comes from fossil fuels (coal, natural gas, petroleum, and other gases),[1] of which 48 pct is from coal. Energy security initiatives in 21st century combined with design requirements to lower carbon dioxide (CO_2) emissions, are pushing the adoption of advanced ultra-supercritical (A-USC) coal power plants with increased steam temperature that promise to increase efficiency.[2] For example, an increase in steam parameters from 566 °C and 24 MPa to 650 °C and 34 MPa would amount to an increase in relative efficiency of 6.5 pct, resulting in a significant decrease in coal use, and hence the reduction of CO_2 emissions.[3] Under the proposed A-USC standards,[2] 9 to 12 wt pct Cr martensitic steels are being considered for thick sections such as the main steam pipe and header in the boiler which will operate up to 650 °C. Within conventional supercritical coal-fired power plants, martensitic steels already operate up to 610 °C. A 40 °C increase in operating temperature requires development of new martensitic steel alloys with higher creep rupture strengths.

Steel alloy discovery today relies on an Edisonian approach with intuitive design choices primarily focused on ppm alloy additions. The 2016 paper by Abe[4] exemplifies this process, where improvement was achieved by alloy additions of V-Nb,[5] later by substituting a part or all of Mo with W,[6] and recently by the addition of Co[7] and B.[8] Initiatives such as Materials Genome Initiative (MGI)[9] and Integrated Computational Materials Engineering (ICME)[10,11] came into prominence in last decade as methodologies to reduce the materials discovery timeline. Aligned with the MGI, this paper presents a data-enabled science approach, focused on leveraging machine learning tools,[12] to improve the creep properties of 9 to 12 wt pct Cr martensitic steels through alloy selection. The aim is to guide the next phase of experiments by gaining insights from previously completed experiments to effectively reduce the time and cost for materials discovery.

Supervised learning is a sub-field of machine learning, which can be broadly defined as any computer program that improves its performance at some task through experience.[13] The metal design machine learning problem can be outlined as: task—search the compositional space for maximum lifetime of martensitic steels at 650 °C; performance measure—uncertainty in

AMIT K. VERMA and JENNIFER L.W. CARTER are with the Department of Materials Science and Engineering, Case Western Reserve University, Cleveland, OH 44106. Contact e-mail: jennifer.w.carter@case.edu JEFFERY A. HAWK is with the National Energy Technology Laboratory, Albany, OR 97321-2198. LAURA S. BRUCKMAN and ROGER H. FRENCH are with the Department of Materials Science and Engineering, Case Western Reserve University and also with the SDLE Research Center, Case Western Research University, Cleveland, OH 44106. VYACHESLAV ROMANOV is with the National Energy Technology Laboratory, Pittsburgh, PA 15236-0940.

Manuscript submitted November 28, 2018.
Article published online April 29, 2019

predictions; and training experience—creep and tensile test data. For supervised learning, a model predicts (estimates) an output based on one or more inputs. Supervised learning has proven to be an effective alternative to computationally expensive physical models in a wide variety of materials research problems.[12,14–16] The paper focuses on the simplest form of supervised learning - linear regression, which exemplifies the process and sets the foundation for more complex supervised learning forms. Although linear regression modeling is simplest of all the methods, it has distinct advantages in terms of inference and, on real-world problems, is often more interpretable in relation to non-linear methods.[17] The objective is to make design choices to select the next material chemistry to increase the creep lifetime to 10^5 hours or greater when alloys are subjected to 100 MPa and 650 °C.

II. HISTORICAL MICROSTRUCTURE DESIGN

The development of 9 to 12 wt pct Cr steels in the twentieth century is described in Reference 18 and particularly in Reference 4 for the last two decades. Important aspects of these descriptions as they pertain to the design of creep resistant microstructures are presented below. The alloying specifications ensure a fully martensitic tempered microstructure. Heat treatment process comprises a solution-annealing treatment (or normalization), a quench to form martensite, followed by a tempering treatment. Solution heat treatment takes place between 900 °C to 1250 °C (depends on chemistry) with holding times between 0.5 to 15 hours. Tempering is carried out between 600 °C and 820 °C, for annealing times of 0.5 to 25 hours depending on material thickness.

A. *Tempered Martensitic Microstructure*

The tempered martensitic microstructure of 9 to 12 wt pct Cr steels is a hierarchical structure containing packet, blocks, and lath boundaries (collectively as sub-boundaries), along with prior-austenite grain boundaries (PAGBs), with a high density of dislocations, and fine precipitates dispersed along the boundaries and in the matrix. $M_{23}C_6$ carbide (M = Cr, Fe), MX carbonitride (M = V, Nb and X = C, N) and Fe_2M Laves phase (M = W, Mo) are the most common precipitates. The $M_{23}C_6$ and MX forms during tempering, and tempering parameters are such that the propensity of the system to form Fe_2W and Fe_2Mo is negligible during tempering treatment.[19] Therefore, Laves phase forms during creep exposure in operation. The dislocation substructure along with $M_{23}C_6$ and MX particles collectively provide obstacle to dislocation motion, which governs the creep rate and rupture life at elevated temperatures.[20]

B. *Loss of Creep Rupture Strength*

The family of 9 to 12 wt pct Cr steels do not exhibit steady state creep rates due to microstructural evolution during creep deformation. The $M_{23}C_6$ carbides, MX carbonitrides, and Laves phase coarsen during creep; coarsening is greater in the vicinity of PAGBs than within grain interiors because of enhanced diffusion path along the PAGBs.[21] The localized loss of precipitation hardening allows for the subsequent coarsening of the lath and block boundaries, resulting in the loss of sub-boundary hardening.[20] The sub-grain width increases as sub-grains transform from elongated to equiaxed sub-grains and the free dislocation density within sub-grains decreases with increased creep deformation.[22,23] Finally, the long-term stability breaks down with the precipitation of a complex Z-phase nitride (Cr(V,Nb)N) which consumes remaining MX carbonitrides[24,25] and deprives the microstructure of fine MX pinning particles.

C. *Microstructure Design Approach*

The design approach targets four attributes (or responses) in an hierarchical manner: (1) sub-grain structure; (2) dislocation density; (3) pinning particles; and (4) diffusion coefficient. At the highest level, compositions are selected to promote the formation of a fine sub-grain martensitic microstructure. Martensitic transformation strain governs the sub-grain structure, where density of dislocations introduced during martensitic transformation primarily determines the subsequent sub-grain size. Large transformation strain, promote a high transformation driving force, and an austenitic phase with high solid solution strengthening surrounding martensite domains are required for making this fine sub-grain structure.[26] Second, mobile dislocation density within sub-grains governs the extent of primary creep regime (or strain to minimum creep rate), where mobile dislocation density increases with decrease in tempering temperature[20] and results in a longer primary creep regime. Third, since high dislocation density enhances quick recovery, dispersion of strong pinning particles becomes necessary to keep the fine sub-grain structure. The stability of the pinning particles is determined by the diffusion coefficient and solubility of elemental species in the different phases. Therefore, fourth, lower diffusion coefficient results in longer stability times.

Self-diffusion coefficients decrease with para- to ferro-magnetic state below the Curie temperature T_c,[27] and are thus inversely proportional to the T_c of the material. The removal of Ni, Si, and Mn, or addition of Co decreases diffusion coefficient by increasing T_c of the material.[20,28] The coarsening of pinning particles is low when diffusion coefficient and equilibrium mole fraction of M atoms in ferrite is low (Ostwald Ripening). For $M_{23}C_6$, reduction of Ni and Mn is required to reduce the diffusion coefficient. Also, presence of B in W containing steels contributes towards high density of $M_{23}C_6$.[8,23] The coarsening rate of MX carbonitrides is very low due to low solubility of Nb and V in ferrite matrix.[29] The MX carbonitride is not an equilibrium phase, and Z-phase forms at the expense of MX particles; although, the formation can be delayed by reducing Nb and Cr (<10 wt pct[25]) concentration.[30,31] Finkler and Schirra[32] empirical relation suggest

changes to alloy composition for low martensite-start (M_S) temperature, although direct effect of composition optimization and various heat treatment combinations on boundary-design, refinement of PAGBs and final martensitic sub-boundaries, have not been explored in full details.[33]

III. METHODS

A. *Data*

Data used for the analysis come from MatNavi database provided by National Institute for Materials Science (or NIMS), Japan.[34–42] The collected data make up two aspects of the material: tensile and creep properties, and how each changes with test environment and processing parameters such as sample chemistry and heat treatment. Distinct groups emerged within the compositional space as the result of t-distributed stochastic neighbor embedding (or t-SNE) cluster analysis[43] (Section III–B). Subsequently, each group was assigned a label by following the naming conventions[44] used by researchers (Table I). The tensile dataset contains a total of 721 observations of yield strength (YS) measured at test temperatures ranging from room temperature to 800 °C. The creep dataset contain a total of 1737 observations of rupture time (RT) measured at multiple stress levels (10 to 517 MPa) and test temperatures (450 °C to 750 °C).

B. *Visualization Using t-SNE: Cluster Labels*

T-distributed stochastic neighbor embedding (t-SNE) is a means of visualizing the similarities between objects of N-dimensional space in a 2-dimensional scatterplot.[43] The technique uses Barnes-Hut approximations,[45] allowing it to be applied on large real-world datasets. The main advantage of t-SNE is its ability to preserve local structure. This means, roughly, that points which are close to one another in the high-dimensional data set will cluster with one another in the 2-dimensional setting. The algorithm models the probability distribution of neighbors around each data point. Here, the term neighbors refers to the set of data points which are closest to the reference data point. In the original, high-dimensional space this is modeled as a Gaussian distribution. In the 2-dimensional output space this is modeled as a t-distribution. The goal of t-SNE is to find a mapping onto the 2-dimensional space that minimizes the differences between these two distributions over all points.

For this work, the R language[46] package "Rtsne" developed by Krijthe[47] is applied. Within the designed function, the main parameter controlling the fitting is called perplexity. Perplexity is equivalent to the number of nearest neighbors considered when matching the original and fitted distributions for each point. A low perplexity means that we care about local scale and focus on the closest other points. High perplexity takes more of a big picture approach. To search for inherently similar groups within the compositional space, t-SNE algorithm provided the stable clusters with a perplexity factor of 3. For this study, compositional variable ranges were normalized (*i.e.*, to rescale the range to 0 to 1) to avoid artificially biasing the visualization for variables with large numeric range. This was conducted because historical inference indicates that in many cases alloying additions in the ppm range are often as important as alloying additions in the many wt pct range.

C. *Change Point Detection*

The change-points are defined as points where there are two different linear relationships in the data that converge to produce a sudden, sharp change in slope. These abrupt changes in slope are often associated with a mechanism change in materials science (*e.g.*, a change from a dislocation mediated plasticity process to a diffusion mediated plasticity process). This change point requires that the phenomena should be described with a piece-wise regression. In R,[46] segmented package[48] uses maximum likelihood to fit a piece-wise model where method constrains the segments to be (nearly) continuous.[49] The function takes a generic linear model and a starting value of the breakpoint (a best-guess estimate) as its arguments, and iteratively varies these parameters to get the best fit by minimizing the gap between the two segments.

D. *Linear Regression: Contributor Subset Selection*

The empirical models for this study utilize linear regression supervised learning approach. The approach involves identifying a subset of the predictors (contributors) which contribute to the maximum variation in the response.[17] For this study, predictors are the set **x**: material composition (Table I) and test environment (temperature and applied stress), and the responses are the set **y**: yield strength (YS) and rupture time (RT). The leaps package[50] in R language[46] performs an exhaustive search for the best subsets of the predictors in **x** for predicting **y** in linear regression, using an efficient branch-and-bound algorithm.[51] The algorithm returns a best model for each size, starting with a single predictor to the maximum number of available predictors. The algorithm can incorporate statistical measures such as Akaike information criterion (AIC), Bayesian information criterion (BIC), or adjusted-R^2 (adj-R^2) for choosing the best model of each size. For the study, adj-R^2 was used for subset selection. The subset selection process does not penalize for model complexity. Therefore, it requires secondary steps to take account of issues such as over-fitting and under-fitting. These secondary steps involve the study of trade-off between bias and variance, which guides the selection of number of predictors needed to minimize over-fitting and under-fitting.[52]

Table I. Compositions of 9 to 12 wt pct Cr Martensitic Steels Used in the Analysis

Labels	C	Cr	Mn	Si	Ni	Mo
9Cr-1Mo	0.09 to 0.13	8.46 to 9.15	0.38 to 0.50	0.34 to 0.86	0.047 to 0.12	0.93 to 1.05
9Cr-2Mo	0.05	9.04	0.5	0.28	0.11	2.03
9Cr-1Mo-V-Nb	0.08 to 0.11	8.31 to 8.74	0.35 to 0.49	0.24 to 0.38	0.04 to 0.28	0.89 to 0.99
9Cr-1.5Mo-V-Nb-B	0.16 to 0.18	9.11 to 9.29	0.05 to 0.06	0.08 to 0.10	0.08 to 0.09	1.54 to 1.57
9Cr-1.5Mo-Co-V-Nb-B	0.12 to 0.14	9.28 to 9.31	0.31 to 0.34	0.08 to 0.09	0.15	1.51 to 1.54
9Cr-Mo-1.8W-V-Nb-B	0.098 to 0.11	9.26 to 9.50	0.41 to 0.42	0.10 to 0.29	0.13 to 0.17	0.36 to 0.42
12Cr	0.12 to 0.14	11.64 to 12.38	0.42 to 0.71	0.21 to 0.50	0.15 to 0.45	0.04 to 0.21
12Cr-1Mo-1W-Co-V-Cu	0.19 to 0.25	11.00 to 12.90	0.55 to 0.87	0.30 to 0.53	0.64 to 0.90	0.91 to 1.22
12Cr-Mo-1.8W-V-Nb-Cu-B	0.11	12.10	0.59	0.27	0.33	0.34
10.5Cr-1Mo-1W-V-Nb	0.12 to 0.15	9.94 to 10.44	0.41 to 0.55	0.05 to 0.07	0.67 to 0.77	0.97 to 1.10
10.5Cr-Mo-2W-V-Nb-Cu-B	0.12 to 0.13	10.65 to 10.73	0.60 to 0.63	0.24 to 0.31	0.32 to 0.36	0.33 to 0.38

Labels	W	Nb	V	B	N	Co	Cu
9Cr-1Mo					0.0154 to 0.023		0.02 to 0.08
9Cr-2Mo		0.006	0.01		0.021		0.02
9Cr-1Mo-V-Nb		0.048 to 0.09	0.185 to 0.23		0.042 to 0.059		0.012 to 0.032 (NA)
9Cr-1.5Mo-V-Nb-B		0.055 to 0.059	0.26 to 0.29	0.0082 to 0.0088	0.014 to 0.019		
9Cr-1.5Mo-Co-V-Nb-B	0.005 (NA)	0.050 to 0.052	0.19 to 0.20	0.0091 to 0.0096	0.016 to 0.026	1.25 to 1.33	0.02 (NA)
9Cr-Mo-1.8W-V-Nb-B	1.67 to 1.74	0.057 to 0.062	0.16 to 0.19	0.002	0.0462		
12Cr					0.0137 to 0.0393		0.03 to 0.21
12Cr-1Mo-1W-Co-V-Cu	0.90 to 1.13		0.21 to 0.30		0.015 to 0.032	0.04 to 0.15	0.03 to 0.15
12Cr-Mo-1.8W-V-Nb-Cu-B	1.82	0.06	0.19	0.003	0.066		0.82
10.5Cr-1Mo-1W-V-Nb	0.97 to 1.00	0.04 to 0.05	0.17 to 0.20		0.041 to 0.055	0.02 (NA)	
10.5Cr-Mo-2W-V-Nb-Cu-B	1.87 to 1.97	0.050 to 0.056	0.19 to 0.22	0.0024 to 0.0039	0.054 to 0.072		0.85 to 0.97

Elements such as Al, P, and S are not included in the table and units are in wt pct. NA represents that some of the samples within the label do not contain the element.

E. *Lasso Regression*

The subset selection process is discrete in nature, and often suffers from high variance.[52] The lasso regression estimate generalized linear models with convex penalties, which makes the process continuous and less susceptible to high variance.[52,53] In 1970, Hoerl and Kennard paper[54] showed that coefficient estimates based on minimum of residual sum of squares suffers if predictors are dependent (or non-orthogonal). In response, they introduced ridge trace to show these effects and to obtain estimates with smaller mean square error by controlling the inflation and general instability associated with least square estimates. Later (1996), Tibshirani[55] introduced lasso regression with lasso penalty ($\sum_{j=1}^{p} |\beta_j| \leq t$) (or "least absolute shrinkage and selection operator") to shrink some coefficients and make other coefficients zero. It retains the features of ridge regression and gives an automatic variable selection effect. Mathematically, lasso regression adds a lasso penalty to the loss function, and the loss function becomes

$$\min_{\beta} \left\{ \frac{1}{2} \sum_{i=1}^{N} \left(y_i - \beta_0 - \sum_{j=1}^{p} x_{ij} \beta_j \right)^2 + \lambda \sum_{j=1}^{p} |\beta_j| \right\} \quad [1]$$

where λ controls the amount of shrinkage, N is total number of samples, each consisting of p predictors, and, y_i (outcome) and x_{ij} are the values for the ith case for loss function. In R language, glmnet package developed by Friedman *et al.*,[53,56] performs lasso regression using cyclical coordinate descent methods.[57]

F. *Larson–Miller Parameter*

In 1952, the Larson–Miller parameter (LMP)[58] was introduced for extrapolating the experimental data on creep rupture life. It was based on the contention that the absolute temperature compensated time function should have a unique value for a given material depending only on the applied stress level (σ)[59] (*i.e.*, time and temperature are dependent variables for diffusion mediated processes) such that:

$$\log(\sigma) = \text{func.} \left[T \left\{ C_{LM} + \log(t) \right\} \right] \quad [2]$$

The term $\left[T \left\{ C_{LM} + \log(t) \right\} \right]$ is LMP, where time t could be stress rupture life (hrs) or time to accumulate a certain amount of strain for applied stress σ (MPa). C_{LM} is Larson-Miller (L-M) constant and T is absolute temperature (K). Larson and Miller first proposed that the constant C_{LM} may have a universal value of 20 without any viable explanation for choosing the value. Later, new alloy systems and different atmospheric environments indicated that C_{LM} other than 20 can lead to improved correlation.[59] In 2013, Tamura *et al.*[60] investigated heat-resistant steels and proposed a value of 30 for C_{LM}, while associating large value of C_{LM} with high creep resistance of martensitic steels.

G. *Validation*

The validation of linear models, with contributors as predictors, was done through partition of data into train and test dataset. The train and test dataset was selected randomly in a 80:20 train:test ratio. The test dataset is used to assess whether the trained model captured the general rules within the range of available data. If the model is generic, the error for the test dataset should be close to the error for train dataset. If the model is not over-fitting the data, then the ratio of error for test dataset to train dataset should be close to one. Random selection of test and train dataset was done 1000 times to evaluate a distribution for ratio of error for test to train dataset.

H. *Outliers: Cook's Distance*

There are different methods to detect the outliers, including standard deviation and Tukey's method[61] which use interquartile (IQR) range approach. For a given continuous variable, one easy way is to use boxplot statistics and label data points that fall above and below the 1.5*IQR as outliers. For multivariate models, declaring an observation as an outlier based on a single feature could lead to unrealistic inferences. Cook's Distance,[62] is a method of defining outliers in a multi-variable space. Cook's distance is a measure computed with respect to a given regression model and therefore is impacted only by the variables included in the model. It computes the influence exerted by each observation **i** on the predicted outcome by measuring the change in fitted values for all observations with and without the presence of observation **i** in the regression model. In R language, standard 'stats' package was used to calculate Cook's distance.[46]

IV. RESULTS AND ANALYSIS

A. *Cluster Labels*

Evaluation of t-SNE cluster analysis finds 8 groups (shown in Figure 1). Using past naming conventions 11 labels were assigned instead of 8 by following the presence/absence of elements and their quantities in a manner similar to adopted by researchers in the past.[44] Table I shows these 11 different labels which gives 56 different sample compositions. This means there are three groups, where sample composition is very close to each other but show inherently different properties. The three overlapping pairs: 9Cr-1Mo with 9Cr-2Mo; 9Cr-1.5Mo-V-Nb-B with 9Cr-1.5Mo-Co-V-Nb-B; and, 10.5Cr-Mo-2W-V-Nb-Cu-B with 12Cr-Mo-1.8W-V-Nb-Cu-B are highlighted in Figure 1. All three overlaps show that these samples are different with respect to only one element. This visualization (Figure 1), together with Table I, highlights the limited compositional space present for the study.

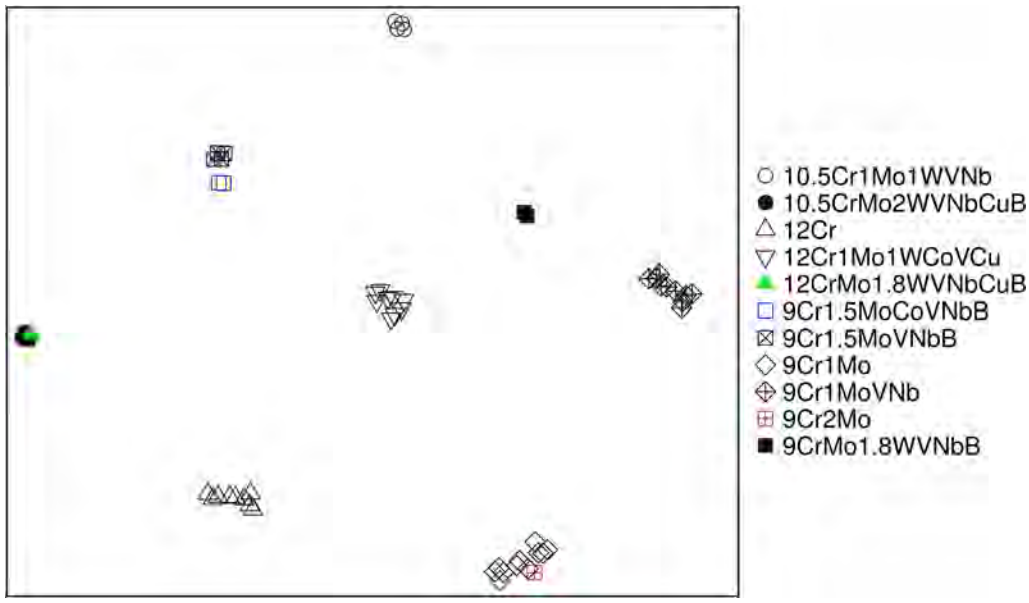

Fig. 1—Visualization of 17-dimension compositional space into 2-dimensional probability space using t-SNE.[43,45,47] Measuring the distances or angles between points in above plot does not give any quantitative information about the data. Description of legends/labels is given in Table I.

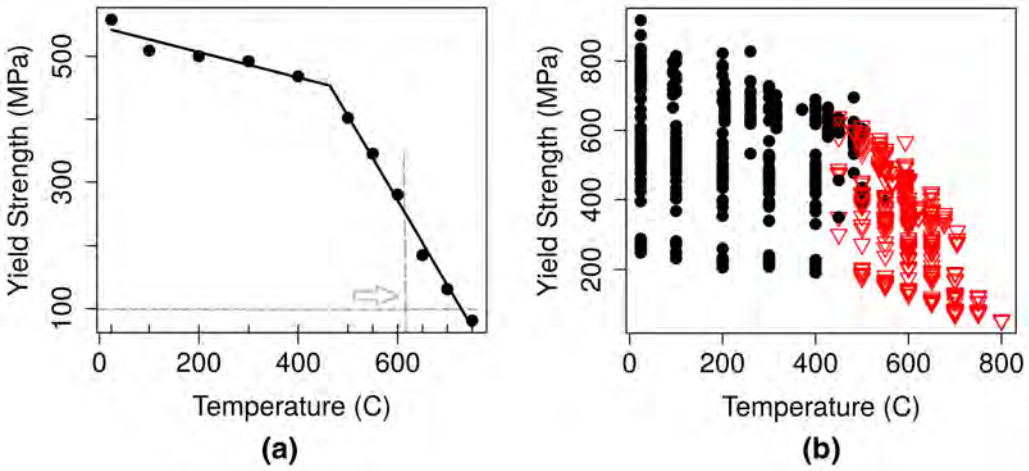

Fig. 2—(*a*) Variation in yield strength (YS) with temperatures for 9Cr1MoVNb label. Dashed line indicates the current operating temperature for 9 to 12 wt pct Cr steels (610 °C) and the standard design stress for application in A-USC plants (100 MPa). The visualization highlights a change point phenomenon associated with mechanism change with increase in temperature. (*b*) Variation in YS with temperature for all the samples. The visualization highlights the separation of data using the change point into high (open triangles) and low (filled circles) temperature regions.

B. *Contributor Subset Selection: Yield Strength*

Figure 2(a) illustrates the change point behavior in the yield strength as a function of test temperature. This change point phenomena is associated with a transition in dominant deformation mechanisms: from athermal dislocation motion to a diffusion mediated dislocation mechanism.[63] With projected operating temperature of 650 °C and above, changes in YS become important as an applied stress greater than YS ($\sigma \geq$ YS) significantly reduces the creep life. The change point phenomenon, as calculated from the tensile strength data, led to the separation of data, using segmented package,[48] into high (open triangles) and low (filled circles) temperature regions for separate evaluation of contributors for different regions (Figure 2(b)).

The spread in the data for a particular temperature in Figure 2(b) shows the variation in YS due to variation in compositional space. To capture this variation, subset selection using leaps package[50] was applied for both temperature regions and the results are tabulated in Table II. On evaluating Cook's distance[62] for both temperature regions, we found no high leverage datapoints (*i.e.*, no outliers). Table II suggests that reducing Si and N, while increasing V and Ni should increase YS for the desired conditions.

Table II. Rank-Ordered Contributors for Yield Strength (YS) at Low and High Temperature Regions

Response	#	Temp						Adj-R^2
YS	389	Low	-Si	-Temp	Cr	V	-Cu	0.89
YS	332	High	-Temp	-Si	V	Ni	-N	0.90

Coefficient of temperature (Temp) changes from − 0.30 to − 1.30 with change point (low to high temperature). Adj-R^2 measures the proportion of variance explained by the contributors, adjusted for the number of independent contributors.

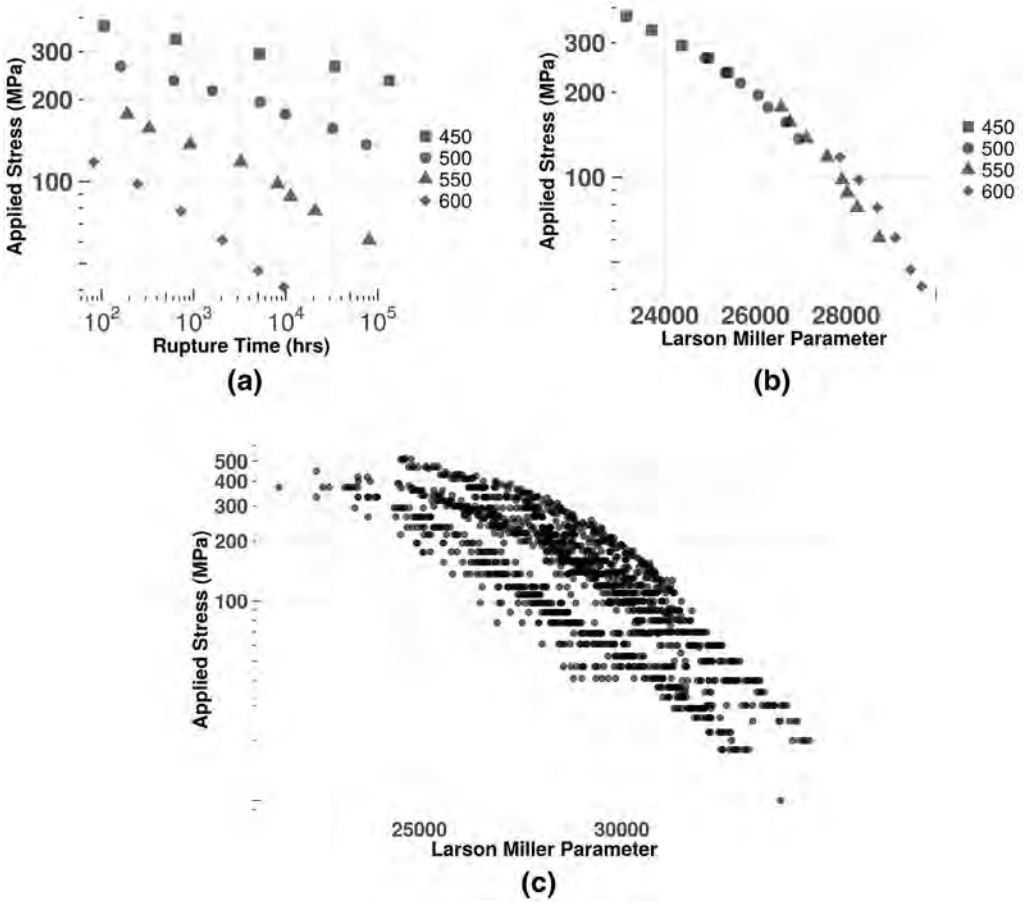

Fig. 3—(*a*) Variation in rupture time with applied stress (σ) at different temperatures (°C) for a single composition (12Cr Label). (*b*) Variation in Larson–Miller parameter (LMP) with σ for the same sample (12Cr label) with an adj-R^2 value of 0.99 for a quadratic fit. The visualization highlights the empirical dimensionality reduction. (*c*) Variation in LMP with σ for all the samples (1737 observations).

C. *Contributor Subset Selection: Rupture Time*

The visualization of RT with σ on a log-log scale is shown in Figure 3(a). Using LMP with $C_{LM} = 30$,[60] the 4 different curves at different temperatures in Figure 3(a) collapse into a single curve (Figure 3(b)). This eliminates one of the two independent variables (test temperature) that can be controlled during a creep test and allow a simple quadratic fit between σ and LMP. Including other compositions gives Figure 3(c), where spread in the data is due to variation in compositional space. The subset selection using leaps package[50] was applied to map the contributors to the RT and the LMP, and the results are tabulated in Table III. On evaluating Cook's distance,[62] we found no high leverage datapoints, *i.e.*, no outliers. Table III suggests that increasing Nb, W, Mo, Ni, B will increase RT and LMP. The increase in adj-R^2 from RT model to LMP model by 28 pct shows the benefit of variable transformations and dimensionality reduction.

The LMP model with the high adj-R^2 is good for predictions, but has limited usability due to the assumption that the mechanisms do not change with temperature. For example, model suggests that increasing Mo will increase LMP, ergo increases RT, irrespective of the temperature, while domain knowledge indicates that the role of Mo and some other elements changes with temperature.[25] To add further insights to the design challenge, we evaluated temperature specific models for RT. This eliminates the high dependency between creep stress and creep temperature (correlation coefficient of -0.75) and focuses on the alloy compositional design variables. A linear fit was assumed between the $\log_{10}(\sigma)$

Table III. Rank-ordered Contributors for Larson–Miller Parameter (LMP) and Rupture Time ($\log_{10}$(RT)) for All Creep Data

Response	#								Adj-R^2
$\log_{10}$(RT)	1737	$-\log_{10}(\sigma)$	–Temp	Nb	W	Mo	Ni	B	0.66
LMP	1737	$-\log_{10}(\sigma)$	$-(\log_{10}(\sigma))^2$	Nb	W	Mo	Ni	B	0.94

Represents the number of observations. Adj-R^2 measures the proportion of variance explained by contributors, adjusted for the number of independent contributors.

Table IV. Temperature (Temp) Specific Rank-Ordered Contributors for Rupture Time ($\log_{10}$(RT))

Temp (°C)	#							Adj-R^2
500	200	$-\log_{10}(\sigma)$	V	W	Mo	–Mn		0.70
550	349	$-\log_{10}(\sigma)$	V	Mo	Cr	–C		0.70
600	327	$-\log_{10}(\sigma)$	Nb	W	Mo	Ni	Co	0.80
650	261	$-\log_{10}(\sigma)$	Nb	W	Mo	Co	−B	0.86
700	127	$-\log_{10}(\sigma)$	V	W	−Cr			0.92

Represent the number of tests/observations conducted for a specific temperature. Adj-R^2 measures the proportion of variance explained by contributors, adjusted for the number of independent contributors.

Table V. Temperature Specific Rank-Ordered Contributors for Rupture Time ($\log_{10}$(RT)) After Correction with Lasso Regression

Temp(°C)	#							Adj-R^2
500	200	$-\log_{10}(\sigma)$	V	W	Mo	–Mn		0.70
550	349	$-\log_{10}(\sigma)$	V	Mo	Cr	–C		0.70
600	327	$-\log_{10}(\sigma)$	Nb	W	Mo	Ni	Co	0.80
650	261	$-\log_{10}(\sigma)$	Nb	W	Mo	Co		0.85
700	127	$-\log_{10}(\sigma)$	V	W	-Cr			0.92

Represent the number of tests/observations conducted for a specific temperature. Adj-R^2 measures the proportion of variance explained by contributors, adjusted for the number of independent contributors.

Table VI. Ratio for Test to Training Error for Different Models, Computed Over 1000 Different Random Allocations of Test and Training Dataset

Response	Temp(°C)	# Training	# Test	Adj-R^2	Ratio
YS	High	265	67	0.90	1.06 ± 0.24
$\log_{10}$(RT)	All	1389	348	0.66	1.02 ± 0.13
LMP	All	1389	348	0.94	1.00 ± 0.07
$\log_{10}$(RT)	500	160	40	0.69	1.10 ± 0.28
$\log_{10}$(RT)	550	279	70	0.70	1.06 ± 0.24
$\log_{10}$(RT)	600	261	66	0.79	1.07 ± 0.25
$\log_{10}$(RT)	650	208	53	0.85	1.06 ± 0.26
$\log_{10}$(RT)	700	101	26	0.92	1.20 ± 0.48

Test/Training represent the number of observations in test/training dataset. Adj-R^2 measures the proportion of variance explained by contributors, adjusted for the number of independent contributors.

and $\log_{10}$(RT) for the calculation of temperature specific contributors. This led to the division of data with respect to temperature, thus reducing the number of observations available for subset selection for a specific temperature model. This reduced data lack variation both in compositional and environmental space, which may induce bias in subset selection process. To mitigate the bias, all temperature subsets with less than 100 observations were removed from the calculation of temperature specific contributors. This brought down the data under study from 1737 to 1264 observations for RT (∼ 73 pct of data). Further, to check for bias, Cook's distance for different temperature specific models was evaluated, and no high leverage data points were found. The contributors are tabulated in Table IV.

D. *Correction with Lasso Regression*

All models presented in Tables II to IV were corrected with lasso regression to mitigate the effect of dependent predictors. First, lasso regression was applied to pick one of the dependent predictor and discard the other for

each model. Second, subset selection was applied to the remaining predictors for each model. This correction confirmed the absence of dependent predictors in Tables II and III, while showing B as dependent predictor in temperature specific model for RT at 650 °C. The correction gave Table V for temperature specific models.

E. *Validation*

The validation of linear models, with contributors as predictors, was done through partition of data into train and test dataset and looking at the ratio of errors. Table VI shows that the ratio is close to one for most cases, and the mean increases with decrease in number of available observations for training and testing of the model. While this ratio is a strong indicator for over-fitting, it can not provide any information about the under-fitting. The under-fitting was assessed during the subset selection process through increase in adj-R^2 with each addition of predictor.

V. DISCUSSION

The motivation behind the study is to provide compositional design insights for the next generation of creep resistant 9 to 12 wt pct Cr steels. This can be translated to (1) identifying which elements are contributing to creep properties, (2) whether their amount should be decreased or increased (qualitative estimates), and (3) by how much (quantitative estimates). The first two aspects have been attempted in previous section. In this section, we'll evaluate the results and move towards quantitative estimates.

A. *Inadequacy of Data*

To make quantitative design choices in composition, limitations that the data provide to conduct statistical analysis must be discussed. For example, linear regression assumes that the observations are normally distributed and predictors are independent, which is not the case for all predictors under study. While dependency between predictors was addressed through lasso regression, other assumptions are assessed though visualization of residuals[64] and its homoscedasticity. Residual plots were observed for all nine models and plots showed that all models, except the temperature specific models for RT, are unbiased. We'll come back to temperature specific models in next section (Section V–B). The absence/presence of alloying elements also show the evolution of 9 to 12 wt pct Cr steels with time.[44] The historical data from multiple independent sources collectively do not strictly follow any statistical assumptions (*e.g.*, homoscedasticity). For example, replacing Mo with W[6] and addition of B[21] were done at the same time to the sample composition. If all the reported data are an attempt to maximize the lifetime of martensitic steels, then the assumption suggests that the data are inadequate for data-driven modeling because it does not contain negative design space. This argument raises pedagogical questions about the collection and reporting of data for the broader scientific community, if the results are to be used in the future for data-driven models.[65] Low adj-R^2 values in Table V, along with bias in residual plots, highlights the absence of microstructure data and suggests that the linear models are at high bias—low variance end (under-fitting of data). In conclusion, historical data are biased, but may provide design insights if the bias can be identified.

B. *Bias in Temperature Specific Models*

An important assumption implicitly made during the splitting of data for temperature specific models is that the data are distributed homogeneously for all temperatures. This assumption is not true, which had been elaborated in Section V–A. This informs that the contributors are biased due to the availability of data points for a specific temperature. In this section, we'll look at the contributors of the temperature specific models to understand the bias and to collect design insights from models.

1. *Role of Cr*

Cr content is needed to attain sufficient oxidation resistance above 600 °C, while high amount of Cr also translates to high amount of $M_{23}C_6$ carbides, which coarsen during service. Figure 4 shows the effect of Cr content on long-term stability. All groups exhibit change point phenomena and an increase in slope, leading to a sharp decline in creep rupture strength. At small RT, high σ, the functional relationship between σ and RT is independent of Cr concentration. This indicate that microstructure evolution for low RT is independent of amount of $M_{23}C_6$ carbides. At large RT, slope changes with Cr concentration, and thus, depends on the evolution of $M_{23}C_6$ carbides. This suggests that high amount of Cr is not desired for long-term stability. Also, element such as Cu is not desired as it was added to 10.5Cr and 12Cr group to suppress the formation of δ-ferrite.

The data in Figure 4 show a rupture life 10^5 hrs at $\geq$ 50 MPa for 9Cr group, while other studies[66] suggest that 9 wt pct Cr does not exhibit sufficient oxidation and corrosion resistance during service at 650 °C. One way

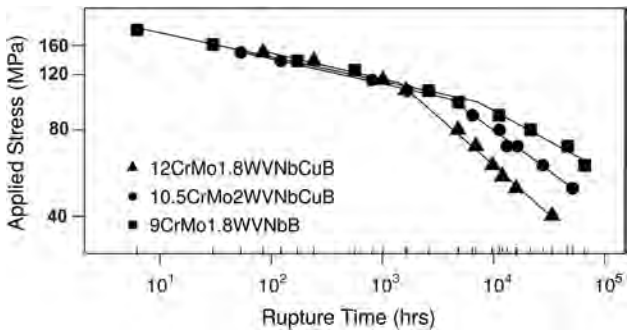

Fig. 4—Effect of Cr content on long-term stability at 650 °C.

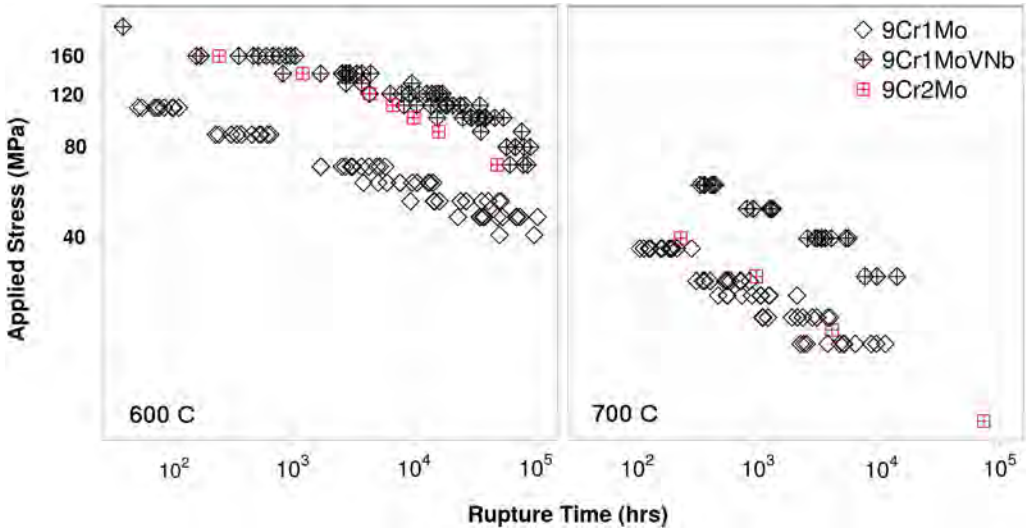

Fig. 5—These figures show the roles of Mo and of V/Nb with temperature. Samples with 9Cr-1Mo-VNb label remain relatively strong over the entire temperature range, while samples with 9Cr-2Mo label, where V and Nb are absent, drops in strength at high temperatures.

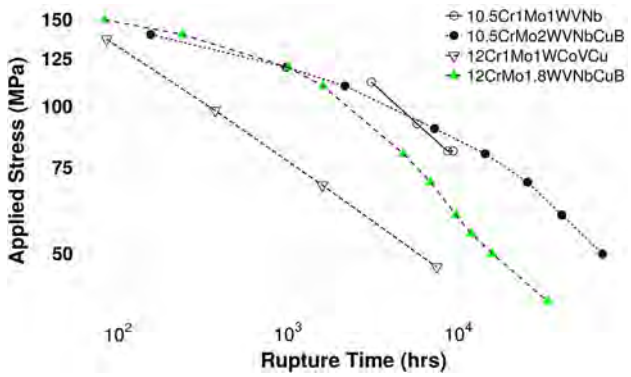

Fig. 6—Role of W/B at 650 °C. Increase in W by reducing Mo, came along with the addition of B, presenting a case of data convolution.

to rectify this issue would be the addition of an element other than Cr (*i.e.*, Si) as another way to enhance oxidation and corrosion resistance. Alternatively, (within the scope of this paper) is to improve 11 to 12 wt pct Cr steels for long-term stability,[67,68] while other is to improve 9 wt pct Cr steels by the application of protective coatings.[69,70]

2. *Role of Mo*

Mo/W provides creep strength through solid solution hardening, until 600 °C. Once Laves phase precipitate at temperatures around 600 °C to 650 °C,[19] matrix gradually loses its solid solution strengthening effect from Mo/W. Then, Laves phase particles contribute through particle strengthening, but improvement diminishes with temperature for Mo-based Laves phase ($(Fe, Cr)_2 Mo$) (Figure 5). At 600 °C, increasing Mo improves creep life, while at 700 °C it does not (Figure 5). This suggests that Mo improves creep life through solid solution strengthening,[25] while it does not provide sufficient precipitation hardening.

3. *Role of V/Nb*

V/Nb form *MX* carbonitrides by combining with N and C.[71] These nano-sized particles (5 to 20 nm in size) form at sub-boundaries and PAGBs, as well as in the matrix.[72] This pins boundaries and dislocations during creep. Figure 5 highlights that the V/Nb strengthens the microstructure over the entire temperature range of collected data (450 °C to 750 °C). This is due to the low coarsening rate of *MX* carbonitrides. In Figure 5, samples with 9Cr-1Mo-VNb label overlaps with samples with 9Cr-2Mo label at 600 °C, while at 650 °C and above, Mo precipitate as intermetallic Laves phase, and we see a drop in samples with 9Cr-2Mo label strength relative to samples with 9Cr-1Mo-VNb label.

4. *Role of W/B*

In the presence of W, the Laves phase particles ($(Fe, Cr)_2 - (Mo, W)$) show high stability,[25,73] which historically led to the substitution of Mo with W.[6] Two examples of this substitution is presented in Figure 6, one for 10.5Cr group and other for 12Cr group. Replacing a part of Mo with W came with the addition of B,[8] which presents a case of data convolution. This convolution, although missed through linear regression subset selection (Table IV), was identified by lasso regression (Table V). Comparison of 12Cr-1Mo-1W-Co-V-Cu label with 12Cr-Mo-1.8W-V-Nb-Cu-B label also suggests that addition of B increases RT at 650 °C. From domain knowledge, we know that very small amount of B significantly improve creep strength by delaying the coarsening of $M_{23}C_6$ carbides.[20] This convolution needs new design experiments to separate the effects of the two elements.

5. *Role of Co*

Co is important to suppress the formation of δ-ferrite with sample containing high amount of ferrite-forming elements, such as Cr and W.[74] This can be expressed in terms of empirically derived linear functions of Ni

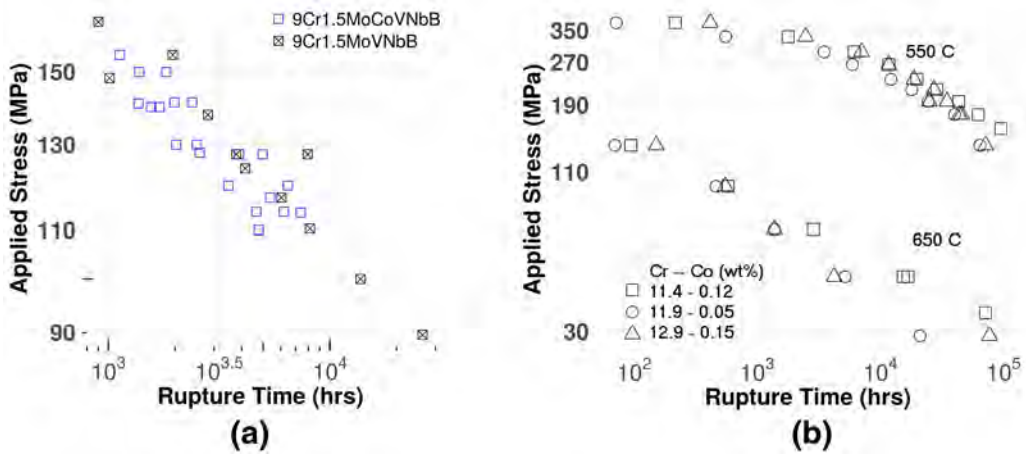

Fig. 7—(*a*) Addition of Co to 9Cr-1.5Mo-V-Nb-B shows no direct effect on creep life (at 650 °C). (*b*) Limited variation of Co within 12Cr-1Mo-1W-Co-V-Cu group shows that Co is beneficial for long-term stability.

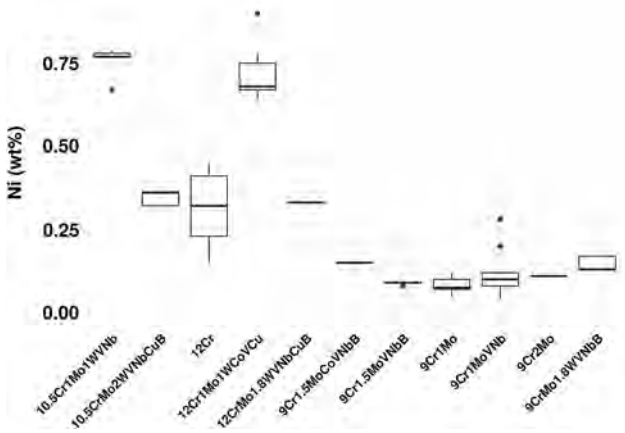

Fig. 8—Variation in Ni across different groups.

equivalent and Cr equivalent, respectively [75]: Cr equivalent = (Cr) + 2(Si) + 1.5(Mo) + 5(V) + 5.5(Al) + 1.75(Nb) + 1.5(Ti) + 0.75(W); Ni equivalent = (Ni) + (Co) + 0.5(Mn) + 0.3(Cu) + 25(N) + 30(C). All elements are expressed in wt pct. The addition of Cu in Figure 4 highlights this balance. Due to limited Co variability available for study, insights are limited. Figure 7 shows two examples from limited available data. Figure 7(a) shows that addition of Co does not effect RT, while Figure 7(b) shows that the presence of Co do improve long-term stability, although the insights are limited as Co is limited to (0.04 to 0.15) wt pct. The domain knowledge informs that the coarsening rate of $M_{23}C_6$ particles and diffusion coefficient decreases with increase in Co concentration and decrease in Ni & Mn concentration,[20,76] therefore, new design experiments are needed to explore the effect of Co.

6. *Role of Ni*

Ni was listed as a ranked contributor in temperature specific model (Table V), as well as in the global model of RT/LMP (Table III) and high temperature YS model (Table II). This contradicts the notion[20,76] that increasing Ni is undesirable for long-term stability, but Figure 8 explains this contradiction. From Figure 8, high Ni content is correlated with increases in Cr and W content. Also, in groups where Cu is present, we see a drop in Ni content. Both of these observations supports the design constraint that increased Cr equivalent elements is balanced with Ni equivalent elements, and explains why Ni is a ranked contributor. The effect of Ni on the diffusion coefficient and replacing it with Co, needs to be examined further.

7. *Summary*

The evaluation under Section V–B provided insights about the effect of different alloying elements in Table V and highlighted bias that was not captured by Lasso regression. In summary, 9 wt pct Cr and V/Nb are desirable for long-term stability, but isolating the effect of V from Nb is limited by data. Although, literature indicates that Nb accelerates the Z-phase formation.[24,25] The role of Mo change with temperature, and it isolates its effect from W. But the addition of B, along with W limits the data interpretation. Similarly, range of Co should be explored and the notion of replacing Ni (for Mn/Cu also) with Co should be examined.

C. *New Compositions*

Identification of bias and new insights in Section V–B, along with the domain study in Section II culminates in a potential design space for new martensitic steels (Table VII). 9Cr steels with high amounts of V, W, and Co over Nb, Mo, and Mn/Ni, respectively, is good for long-term stability at 650 °C, along with low Si for YS. The dependency of B and N is well documented,[63] therefore, special attention must be given to their amounts. A 2016 paper by Abe[4] highlighted three different compositions: MARBN (9Cr-3W-3Co-V-Nb-N-B), low-C 9Cr (9Cr-2.4W-1.8Co-V-Nb), and SAVE 12AD (9Cr-2.9W-Co-V-Nb-Ta-Nd-N), for 650 °C. While all three compositions agree with the results obtained through this study, the role of Co and C, and

Table VII. Data Analytics Predicts That the Following Scope for New Experimental Alloys Should Result in Beneficial Creep Properties

Element	Range	Role	Suggestion (Wt Pct)	Remarks
C	0.05 to 0.25	form	< 0.15	depends on Cr
Cr	8.31 to 12.90	carbides	9.0 to 9.5	excess C is not desired
V	0.15 to 0.30			V is preferred[a]
Nb	0.04 to 0.09	—		between Nb and V
N	0.0137 to 0.072	carbonitrides	0.015 to 0.025	depends on B
B	0.002 to 0.0096	stabilizes $M_{23}C_6$	0.008 to 0.01	Form BN[a] if present in excess
Mo	0.04 to 2.03	form laves	< 0.5	W is
W	0.005 to 1.97	phases	> 1.5	preferred
Mn	0.05 to 0.87			
Ni	0.04 to 0.90	austenite		Co is
Co	0.02 to 1.33	stabilizers		preferred[a]
Cu	0.012 to 0.97			
Si	0.05 to 0.86	impurity		undesired[a]
Al	0.001 to 0.044	getters		
P	0.001 to 0.029	impurity		undesired[a]—as low
S	0.001 to 0.017			as possible

Remarks containing [a]represents that the statement is supported by existing literature, and not through data-driven models.

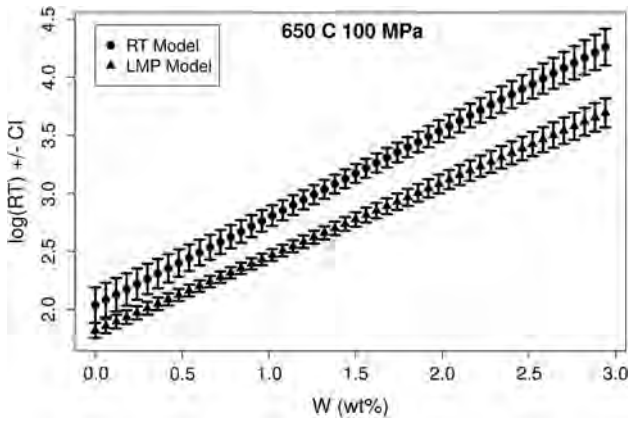

Fig. 9—Change in $\log_{10}$(Rupture Time) (RT), along with confidence intervals (CI) with W at 650 °C, 100 MPa for the base composition of 9Cr-Mo-1.8W-VNb-B label. RT model represents temperature specific model at 650 °C in Table V. LMP model represents LMP global model in Table III.

addition of Ta and Nd, is not captured in data. Also, in compositions proposed by Abe,[4] Mo is absent, Nb is present (despite its effect on Z-phase formation), and B is absent with low C.

Rough estimates of RT and YS, along with confidence intervals,[77] can be obtained through limited linear models. Linear models are not good for predictions; therefore, focus is on what we can infer from these estimates and confidence intervals. Of all the 11 labels (Table I), samples from 9Cr-Mo-1.8W-VNb-B label shows best long-term stability, which narrows down the compositional space for exploration and gives a region to tailor with new insights, particularly the effect of W and Co. The effect of W on RT is evaluated using temperature specific RT model at 650 °C (Table V) and LMP model in Table III, and results are shown in Figure 9. The estimates from both models show that 3 wt pct W by itself would not be enough to provide 10^5hours of rupture life. Therefore, papers published in last 2 to 3 years[78–84] were focused on exploring the combined benefits of Co and W.

VI. CONCLUSIONS

The data-driven approach successfully identifies the major contributors towards creep strength. The visualization using t-SNE, along with manually assigned labels, showed that 56 unique compositions does not contain variability along all 17 elements. This bias supervised the subset selection process and provided major contributors for YS and RT after correction through Lasso regression which eliminated B as a contributor. The LMP model was useful in illustrating the usage of visualization for developing better predictive models, although at the cost of design insights. Its limit is highlighted by the change point analysis indicating that mechanisms are not constant as a function of temperature. The visualization of temperature specific model contributors further elucidated the bias and showed dependencies among elements. All insights collectively, along with domain knowledge, give us suggestions on where to move next for new martensitic steels and are summarized in Table VII. These suggestions align with already proposed compositions by Abe,[4] and show that linear and lasso regression are quite competitive for inference. The study shows gaps in the data through unsupervised learning and visualization, which highlights, not just the regions for better creep strength, but also the regions where new data collection is needed for better predictive models.

ACKNOWLEDGMENTS

This work made use of the High Performance Computing Resource in the Core Facility for Advanced Research Computing at Case Western Reserve University. This project was funded by the Department of Energy (Grant DE-FE0028685), National Energy Technology Laboratory, an agency of the United States Government.

DISCLAIMER

This project was funded by the Department of Energy, National Energy Technology Laboratory, an agency of the United States Government. Neither the United States Government nor any agency thereof, nor any of their employees, makes any warranty, expressed or implied, or assumes any legal liability or responsibility for the accuracy, completeness, or usefulness of any information, apparatus, product, or process disclosed, or represents that its use would not infringe privately owned rights. Reference herein to any specific commercial product, process, or service by trade name, trademark, manufacturer, or otherwise does not necessarily constitute or imply its endorsement, recommendation, or favoring by the United States Government or any agency thereof. The views and opinions of authors expressed herein do not necessarily state or reflect those of the United States Government or any agency thereof.

APPENDIX A: REGRESSION COEFFICIENTS

The rank-ordered contributors presented in Tables II through V represents the fitted equations, minus the magnitude of regression coefficients. For example, rupture time (RT) model in Table III can be translated to:

$$\log_{10}(RT) = \beta_0 - \beta_1 \log_{10}(\sigma) - \beta_2 Temp + \beta_3 \mathrm{Nb} + \beta_4 \mathrm{W} + \beta_5 \mathrm{Mo} + \beta_6 \mathrm{Ni} + \beta_7 \mathrm{B}$$

The magnitude of regression coefficients are a function of magnitude of the associated variable. For example, change in B at ppm level may bring about small changes in response, although being the changes at ppm level will push the magnitude of regression coefficient to a very high value. This might appear to a reader at first glance that changes in B might bring about better results than W or Co. As the focus is on inference throughout the paper, except for Section III–C, the positive and negative signs served the purpose for the results, and avoided the unwanted confusion. Here, we present regression coefficients and their scaled counterparts to show the complete breadth of the fitted models. The scaling was done by subtracting the mean and dividing by the standard deviation of a variable (Table AI through AIV).

Table AI. Rank-Ordered Contributors for Yield Strength (YS) at Low and High Temperature Regions with Regression Coefficients and Their Scaled Counterparts

Response	#	Temp						Adj-R^2
YS	389	Low	Si	Temp	Cr	V	Cu	0.89
			− 282	− 0.29	72.2	1020	− 210	
			− 0.30	− 0.27	0.56	0.62	− 0.25	
YS	332	High	Temp	Si	V	Ni	N	0.90
			− 1.35	− 272	596	113	− 1700	
			− 0.68	− 0.33	0.41	0.20	− 0.19	

Table AII. Rank-Ordered Contributors for Larson–Miller Parameter (LMP) and Rupture Time (RT) for All Creep Data with Regression Coefficients and Their Scaled Counterparts

Response	#								Adj-R^2
$\log_{10}$(RT)	1737	$\log_{10}(\sigma)$	Temp	Nb	W	Mo	Ni	B	0.66
		− 5.14	− 0.025	17.0	0.34	0.82	1.50	138	
		− 1.77	− 1.71	0.58	0.26	0.37	0.42	0.34	
LMP	1737	$\log_{10}(\sigma)$	$(\log_{10}(\sigma))^2$	Nb	W	Mo	Ni	B	0.94
		− 78000	− 6890	20800	585	1200	1730	155000	
		− 36	− 3.2	0.30	0.19	0.24	0.21	0.16	

Table AIII. Temperature (Temp) Specific Rank-Ordered Contributors for Rupture Time ($\log_{10}$(RT)) with Regression Coefficients and Their Scaled Counterparts

Temp (°C)	#							Adj-R^2
500	200	$\log_{10}(\sigma)$	V	W	Mo	-Mn		0.70
		− 7.58	3.32	0.99	0.85	− 1.83		
		− 1.33	0.41	0.56	0.45	− 0.28		
550	349	$\log_{10}(\sigma)$	V	Mo	Cr	–C		0.70
		− 5.80	8.28	1.08	0.28	− 6.46		
		− 1.29	1.03	0.50	0.48	− 0.36		
600	327	$\log_{10}(\sigma)$	Nb	W	Mo	Ni	Co	0.80
		− 5.08	20.8	0.54	0.78	0.99	1.09	
		− 1.13	0.69	0.39	0.32	0.25	0.13	
650	261	$\log_{10}(\sigma)$	Nb	W	Mo	Co	B	0.86
		− 5.17	20.2	0.86	0.68	1.79	− 115	
		− 1.26	0.77	0.72	0.26	0.56	− 0.29	
700	127	$\log_{10}(\sigma)$	V	W	Cr			0.92
		− 5.20	7.02	0.48	− 0.18			
		− 1.31	0.84	0.51	− 0.22			

Table AIV. Temperature Specific Rank-Ordered Contributors for Rupture Time After Correction with Lasso Regression Along with Regression Coefficients and Their Scaled Counterparts

Temp(°C)	#						Adj-R^2
650	261	$\log_{10}(\sigma)$	Nb	W	Mo	Co	0.85
		− 5.10	19.0	0.76	0.83	0.89	
		− 1.24	0.73	0.64	0.32	0.28	

REFERENCES

1. U.S. Energy Information Administration: *What is U.S. electricity generation by energy source*? U.S. Energy Information Administration (EIA) Apr 2017.
2. J. Shingledecker, R. Purgert, and P. Rawls: in *Proceeding the 7th International Conference on Advances in Materials Technology for Fossil Power Plants*, 2013, pp. 41–52.
3. R. Viswanathan and J. Nutting: in *Advanced Heat Resistant Steels for Power Generation: Conference Proceedings*, 27–29 April 1998, San Sebastian, Spain: IOM Communications, 1999.
4. F. Abe: *J. Pressure Vessel Technol.*, 2016, vol. 138 (4), p. 040804.
5. V.K. Sikka: in *Topical Conference on Ferritic Alloys for Use in Nuclear Energy Technologies*, J.W. Davis and D.L. Michel, eds., Snowbird, UT, June 1983, pp. 19–23.
6. F. Abe and S. Nakazawa: *MTA*, 1992, vol. 23 (11), pp. 3025–34.
7. K. Yamada, M. Igarashi, S. Muneki, and F. Abe: *ISIJ Int.*, 2003, vol. 43 (9), pp. 1438–43.
8. T. Horiuchi, M. Igarashi, and F. Abe: *ISIJ Int.*, 2002, vol. 42 (Suppl), pp. S67–71.
9. Materials Genome Initiative for Global Competitiveness: Tech. rep. Jun. 2011.
10. S.M. Arnold, F. Holland, T.P. Gabb, M. Nathal, and T.T. Wong: *The Coming ICME Data Tsunami and What Can be Done*, American Institute of Aeronautics and Astronautics, 2013.
11. S.M. Arnold, F. Holland, and B.A. Bednarcyk: *Robust Informatics Infrastructure Required for ICME: Combining Virtual and Experimental Data*, American Institute of Aeronautics and Astronautics, 2014.
12. K. Rajan: *Informatics for Materials Science and Engineering Data-Driven Discovery for Accelerated Experimentation and Application*, 2013.
13. T.M. Mitchell: *Machine Learning*, 1st ed., McGraw-Hill Education, New York, 1997.
14. H.K.D.H. Bhadeshia: *ISIJ Int.*, 2001, vol. 41 (6), pp. 626–40.
15. H.K.D.H. Bhadeshia: *ISIJ Int.*, 1999, vol. 39 (10), pp. 966–79.
16. I.E. Castelli and K.W. Jacobsen: *Model. Simul. Mater. Sci. Eng.*, 2016, vol. 5, p. 055007.
17. G. James, D. Witten, T. Hastie, and R. Tibshirani: *An Introduction to Statistical Learning*, Springer Texts in Statistics, Springer, New York, 2013, vol. 103.
18. R. Klueh and D. Harries: in: *High-Chromium Ferritic and Martensitic Steels for Nuclear Applications*, R. Klueh and D. Harries, eds., ASTM International, West Conshohocken, PA, 2001, pp. 5–23. 10.1520/MONO10017M.
19. G. Dimmler, P. Weinert, E. Kozeschnik, and H. Cerjak: *Mater. Charact.*, 2003, vol. 51 (5), pp. 341–52.
20. K. Maruyama, K. Sawada, and J.-I. Koike: *ISIJ Int.*, 2001, vol. 41 (6), pp. 641–53.
21. H. Semba and F. Abe: *Energy Mater.*, 2006, vol. 1 (4), pp. 238–44.
22. H. Cerjak, P. Hofer, and B. Schaffernak: *Key Eng. Mater.*, 2000, vol. 171174, pp. 453–60.
23. K. Sawada, M. Takeda, K. Maruyama, R. Ishii, M. Yamada, Y. Nagae, and R. Komine: Mater*Sci. Eng. A*, 1999, vol. 267 (1), pp. 19–25.
24. V. Sklenicka, K. Kuchacova, M. Svoboda, L. Kloc, J. Bursik, and A. Kroupa: *Mater. Charact.*, 2003, vol. 51 (1), pp. 35–48.
25. J. Hald: *Int. J. Press. Vessels Pip.*, 2008, vol. 85 (1–2), pp. 30–37.
26. S.B. Singh and H.K.D.H. Bhadeshia: Mater*Sci. Eng. A*, 1998, vol. 245 (1), pp. 72–79.
27. F.S. Buffington, K. Hirano, and M. Cohen: *Acta Metal.*, 1961, vol. 9 (5), pp. 434–39.
28. B.J. Ganesh, S. Raju, A. Kumar Rai, E. Mohandas, M. Vijayalakshmi, K.B.S. Rao, and B. Raj: *Mater. Sci. Technol.*, 2011, vol. 27 (2), pp. 500–512.
29. J. Lecomte-Beckers, F. Schubert, and P.J. Ennis (Eds.): Materials for advanced power engineering 1998, Abstracts of the 6th Conference: no. v. 4 in Schriften des Forschungszentrums Jülich: Forschungszentrum Jülich, Jülich, Germany, 1998.
30. H.K. Danielsen and J. Hald: *Calphad*, 2007, vol. 31 (4), pp. 505–14.
31. H.K. Danielsen, P.E.D. Nunzio, J. Hald, H.K. Danielsen, and J. Hald: Metall Mater*Trans. A*, 2013, vol. 44A (5), pp. 2445–52.
32. H. Finkler and M. Schirra: *Steel Res.*, 1996, vol. 67 (8), pp. 328–42.
33. X. Zhou, C. Liu, L. Yu, Y. Liu, and H. Li: *J. Mater. Sci. Technol.*, 2015, vol. 31 (3), pp. 235–42.
34. K. Yadi: NIMS Creep Data Sheet (JIS SUS 403-B, 12cr, bar), Tech. Rep. 13B, NIMS, Tokyo, 1994.
35. H. Irie: NIMS Creep Data Sheet (JIS STBA 26, 9cr-1mo, tube), Tech. Rep. 19B, NIMS, Tsukuba, 1997.
36. H. Irie: NIMS Creep Data Sheet (1cr-0.5mo-0.25v and 12cr-1mo-1w-0.25v, bolting material), Tech. Rep. 44, NIMS: Tsukuba 1997.

37. H. Irie: NIMS Creep Data Sheet (JIS SUH 616-B, 12cr-1mo-1w-0.3v, bar), Tech. Rep. 10B, NIMS, Tsukuba 1998.
38. S. Matsuoka: NIMS Creep Data Sheet (KA-STBA 27, 9cr-2mo, tube), Tech. Rep. 46A, NIMS, Tsukuba 2005.
39. NIMS Creep Data Sheet: Tech. Rep. 48A, NIMS, Japan 2012.
40. NIMS Creep Data Sheet (KA-SUS 410 J3, 12cr-2w-0.4mo-1-cu-Nb-V): No. 51a, Tech. rep., NIMS, Japan 2013.
41. NIMS Creep Data Sheet (KA-SUS 410j3 DTB, 12cr-2w-0.4mo-1-cu-Nb-V (Tube)): No. 52a, Tech. rep., NIMS, Japan 2013.
42. NIMS Creep Data Sheet (9cr-1mo-V-Nb): Tech. Rep. 43A, NIMS, Japan 2014.
43. L. V. D. Maaten, G. Hinton: J. Mach. Learn. Res. 2008, 9(Nov), 2579–2605.
44. F. Masuyama: *ISIJ Int*., 2001, vol. 41 (6), pp. 612–25.
45. L.V.D. Maaten: *J. Mach. Learn. Res*., 2014, vol. 15, pp. 3221–45.
46. R Core Team: in *R: A Language and Environment for Statistical Computing: R Foundation for Statistical Computing*, Vienna, Austria, 2017.
47. J. H. Krijthe: *Rtsne: T-Distributed Stochastic Neighbor Embedding using Barnes-Hut Implementation*, R Package version 0.13 2015.
48. V.M. Muggeo: *R News*, 2008, vol. 8 (1), pp. 20–25.
49. V.M.R. Muggeo: *Stat. Med*., 2003, vol. 22 (19), pp. 3055–71.
50. T. Lumley based on Fortran code by Alan Miller: Leaps: Regression Subset Selection, R Package version 3.0 2017.
51. P.M. Narendra and K. Fukunaga: IEEE Trans*Comput*., 1977, vol. 9 (C-26), pp. 917–22.
52. T. Hastie, R. Tibshirani, J. Friedman: in *The Elements of Statistical Learning: Data Mining, Inference, and Prediction*, 2nd edn., Springer Series in Statistics, Springer, New York, 2009.
53. J. Friedman, T. Hastie, and R. Tibshirani: *J Stat Softw*, 2010, vol. 33 (1), pp. 1–22.
54. A.E. Hoerl and R.W. Kennard: *Technometrics*, 1970, vol. 12 (1), p. 55.
55. R. Tibshirani: *J. R. Soc. Ser. B (Methodol.)*, 1996, vol. 58 (1), pp. 267–88.
56. N. Simon, J. Friedman, T. Hastie, and R. Tibshirani: *J. Stat. Softw*., 2011, vol. 39 (5), pp. 1–13.
57. J. Friedman, T. Hastie, H. Höfling, and R. Tibshirani: *Ann. Appl. Stat*., 2007, vol. 1 (2), pp. 302–32.
58. F.R. Larson and J. Miller: *Trans. ASME*, 1952, vol. 74, pp. 765–71.
59. F.T. Furillo, S. Purushothaman, and J.K. Tien: *Scripta Metall*., 1977, vol. 11 (6), pp. 493–96.
60. M. Tamura, F. Abe, K. Shiba, H. Sakasegawa, and H. Tanigawa: Metall*Mater. Trans. A*, 2013, vol. 44 (6), pp. 2645–61.
61. J.W. Tukey: *Biometrics*, 1949, vol. 5 (2), pp. 99–114.
62. R.D. Cook: *Technometrics*, 1977, vol. 19 (1), pp. 15–18.
63. *Creep Resistant Steels*, 1st ed., F. Abe, and R. Viswanathan, and T.-U. Kern, eds., *Creep Resistant Steels*, Woodhead Publishing, Cambridge, 2008.
64. D.C. Montgomery, E.A. Peck, and G.G. Vining: *Introduction to Linear Regression Analysis*, Wiley, New York, 2012.
65. J.A. Knottnerus and P. Tugwell: *J. Clin. Epidemiol*., 2013, vol. 66 (10), pp. 1061–63.
66. H. Nickel, Y. Wouters, M. Thiele, and W.J. Quadakkers: *Fresenius J. Anal. Chem*., 1998, vol. 361 (6–7), pp. 540–44.
67. F. Liu, M. Rashidi, L. Johansson, J. Hald, and H.-O. Andrén: *Scripta Mater*., 2016, vol. 113, pp. 93–96.
68. M. Subanović, J. Pirón, F. Zeller, M. Jarrar, A. Schneider: 2018, V001T01A008.
69. V. Rohr, M. Schütze, E. Fortuna, D.N. Tsipas, A. Milewska, and F.J. Pérez: *Mater. Corros*., 2005, vol. 56 (12), pp. 874–81.
70. Y. Yamamoto, M. P. Brady, G. Muralidharan, B. A. Pint, P. J. Maziasz, D. Shin, B. Shassere, S. S. Babu, C.-H. Kuo: *Development of Creep-Resistant, Alumina-Forming Ferrous Alloys for High-Temperature Structural Use*, American Society of Mechanical Engineers, 2018, pp. V001T04A003.
71. Y. Shen, H. Liu, Z. Shang, and Z. Xu: *J. Nucl. Mater*., 2015, vol. 465, pp. 373–82.
72. F. Abe, T. Horiuchi, M. Taneike, and K. Sawada: *Mater. Sci. Eng. A*, 2004, vol. 378 (1–2), pp. 299–303.
73. F. Abe: *Mater. Sci. Eng. A*, 2004, vol. 387389, pp. 565–69.
74. L. Helis, Y. Toda, T. Hara, H. Miyazaki, and F. Abe: *Mater. Sci. Eng. A*, 2009, vol. 510511, pp. 88–94.
75. G. George, H. Shaikh: in *Corrosion of Austenitic Stainless Steels, Woodhead Publishing Series in Metals and Surface Engineering*, H. S. Khatak, B. Raj, eds., Woodhead Publishing, Cambridge, 2002, pp. 1–36.
76. Y.F. Yin and R.G. Faulkner: Mater*Sci. Eng. A*, 2003, vol. 344 (1), pp. 92–102.
77. J. Neyman: *Phil. Trans. R. Soc. Lond. A*, 1937, vol. 236 (767), pp. 333–80.
78. A.E. Fedoseeva, N.R. Dudova, and R.O. Kaibyshev: *Phys. Metals Metallogr*., 2017, vol. 118 (6), pp. 591–600.
79. F. Abe, T. Ohba, H. Miyazaki, Y. Toda, M. Tabuchi: Mater. High Temp. 2019, 0 (0), 1–11.
80. A. Fedoseeva, N. Dudova, R. Kaibyshev, and A. Belyakov: *Metals*, 2017, vol. 7 (12), p. 573.
81. A. Fedoseeva, N. Dudova, and R. Kaibyshev: *Mater. Sci. Eng. A*, 2016, vol. 654, pp. 1–12.
82. R. Mishnev, N. Dudova, and R. Kaibyshev: *Mater. Sci. Eng. A*, 2018, vol. 713, pp. 161–73.
83. A. Fedoseeva, N. Dudova, and R. Kaibyshev: *J Mater Sci Mar*., 2017, vol. 52 (5), pp. 2974–88.
84. A. Fedoseeva, I. Nikitin, N. Dudova, and R. Kaibyshev: *Mater. Sci. Eng. A*, 2018, vol. 724, pp. 29–36.